

Temporal-lobe Epilepsy: Harmonic and Anharmonic Periodicity in Microelectrode Voltage

François A. Marshall, *Member, IEEE*

© 20xx IEEE. Personal use of this material is permitted. Permission from IEEE must be obtained for all other uses, in any current or future media, including reprinting/republishing this material for advertising or promotional purposes, creating new collective works, for resale or redistribution to servers or lists, or reuse of any copyrighted component of this work in other works.

Abstract—Temporal-lobe epilepsy in humans is often associated with widespread, synchronized neuron firing that co-occurs with traveling waves in local field potential. These traveling waves generate stochastic oscillations in a time series of microelectrode voltage, and previous work has deemed it informative for traveling-wave analysis to study the mean periodicity. This manuscript reveals that: a) mean voltage (i.e., traveling-wave periodicity) adequately explains the observed voltage periodicity only for a select few time intervals during seizure; and b) mean voltage has a 7 Hz cosine-series representation indicative of a nonlinear system response given alpha-rhythm input. The a) result implies that residual noise should be modelled explicitly, while b) motivates a departure from the conventional plane-wave modeling regime in source-localization efforts. The 7 Hz fundamental frequency is unsurprising given the relative transparency of the brain to 14 Hz alpha rhythms in neurophysiological diseases (14 Hz being a subharmonic frequency of the 7 Hz signal).

Index Terms—Alpha periodicity, Epilepsy, Cosine series, Microelectrode array, Multitaper spectral analysis

I. INTRODUCTION

THE electrophysiological manifestation of temporal-lobe epilepsy is high-synchronization spatiotemporal organization of neocortical multiunit firing. When multiunit activity is outstanding, synaptic potential also exhibits stereotyped behaviour: producing traveling waves in local field potential (LFP). This manuscript considers voltage recordings from a microelectrode array (MEA) in a deep-lying neocortical layer¹. In previous literature², the phase of an ictal-discharge traveling wave is used to localize a spherical-wave source.; that is, the signal is assumed a wavepacket³. In [21], the

Submitted January 18, 2023. This work was supported by National Institute of Neurological Disorders and Stroke R01NS110669.

F. A. Marshall completed this work as Postdoctoral Associate (2020-2022) and Visiting Scholar (2022) with Mathematics and Statistics Boston University, 111 Cummington Mall #140C, Boston, MA 02215, United States (e-mail: francois.marshall@queensu.ca).

¹Specific details of this setup are discussed in [29].

²e.g., [5], [21], [29].

³What [9] describes as a narrowband superposition of normal modes that destructively interfere to make the resultant appear as if the superposition of two equal-amplitude, different-frequency plane waves.

spatiotemporal LFP model is refined: the traveling-wave periodicity is thought to approximate steady-state dynamics of a Turing-Hopf dynamical system with stochastic forcing. To this end, the wavepacket represents time-evolutionary mean MEA voltage whose normal modes have high signal-to-noise ratio (SNR).

This manuscript introduces a cosine-series model for mean MEA voltage. In assuming a nonlinear system function, the new model departs from the wavepacket modeling convention because: a MacLaurin polynomial whose argument is a neural rhythm⁴ can have large enough order that the normal modes of the system-response function are highly dispersed across the nonnegative half of the principal domain. An advantage of the new model is that it admits nonlinearity and stochastic periodicity that are realistic qualities of the underlying cortical dynamics. To this end, the identified normal modes are less likely to be spurious signal elements than in the wavepacket model. This manuscript discusses the results of a novel multitaper spectral analysis of MEA-voltage data, accounting for the time evolution of voltage periodicity during the course of a human seizure.

All code and results used for the analysis of this manuscript can be found at the code repository of [17]. There at that repository can be found a useful `README.docx` file, which itself makes reference to that important instructions document which is referenced here as [16]. The remainder of this section presents the model. Then Section II presents a longitudinal analysis for one human-subject / MEA-electrode element of the complex survey. The analysis reveals: how the periodicity of mean voltage specifies a partition of the voltage record during seizure into four epochs (Section II-A); and convincing evidence for a 7 Hz fundamental frequency of the cosine series (Section II-B). Finally: the discussion proposes a nominal biophysical mechanism to explain the source of periodicity for two of the epochs, while motivating further work to understand mechanisms responsible for the other two epochs (Section III).

For $\Delta t > 0$ a sampling period and $x : \mathbb{R} \rightarrow \mathbb{R}$, the time series, $\mathbf{x} \in \mathbb{R}^N$, of MEA-voltage is given by

$$\mathbf{x}^T = [x(t_n)]_{n=0}^{N-1}, \quad (1)$$

where, for $n \in \mathbb{Z}$: the n 'th time, t_n is given by

$$t_n = n \cdot \Delta t. \quad (2)$$

⁴Here, a neural rhythm is thought to be a nonrandom, narrowband L^2 -signal that has a cosine-series expansion.

Model x by the generative random vector, \mathbf{X} , where⁵

$$\mathbf{X}[n] = X \left(\frac{t_n}{T_N} \right), \quad (3)$$

with the terms given as follows.

- 1) X is a real-valued L^p -process on \mathbb{R}^6 , where $p \in \mathbb{N}_{>1}$.⁷
- 2) T_N is the record length, where $T_N = t_{N-1}$.

The MEA-voltage has the signal-plus-noise decomposition,

$$X = x^{(SGN)} + X^{(NSE)}, \quad (4)$$

where $x^{(SGN)}$ and $X^{(NSE)}$ respectively denote the mean signal (SGN) and noise (NSE). Denote by J_{SGN} the order of the cosine series.

In this manuscript, the data considered comprise a 30 kHz voltage series from a single MEA electrode and have been drawn from a complex clinical survey of neocortical seizure activity. Details of the survey can be found in [29], while the data are available at [28]. The electrode having unit identification index is considered from the Subject C5 study (refer to Table 1 in [29] for details).

II. RESULTS

A. The Time-evolutionary Periodicity of Microelectrode Voltage

For a survey of time sections, preliminary MEA-voltage multitaper power-spectral and harmonic analyses reveal for $x^{(SGN)}$ -reconstructions how a sparse cosine-series signal can explain the X mean signal. Fig. 1 presents the following.

- 1) First column:
 - x (black, $|\Delta t|^{-1} = 3 \times 10^4$, $N = 6 \times 10^4$).
 - An $x^{(SGN)}$ -reconstruction (grey)⁸.
- 2) Second column: A reconstruction of the expected value of

$$X^{(NSE)} \parallel \{X = x\}.$$

In each plot row of Fig. 1, the 30 kHz trace (x) exhibits periodicity stereotypical of one of four epochs. Table I displays how each plot row indicates the dominance of one or the other of $x^{(SGN)}$ and $X^{(NSE)}$ during the considered section window. The table includes rows entitled ‘‘Alpha periodicity’’ because - in the corresponding epochs - the fundamental frequencies of the $x^{(SGN)}$ cosine series are 7.2 Hz and 21.9 Hz, respectively; both are approximately mode frequencies of a 7 Hz cosine series⁹. Yet stronger evidence for the 7 Hz hypothesis is that the

⁵For 3, the notation of T_N^{-1} in the X argument is a reminder that t_n enters as $t_n \cdot T_N^{-1}$ in any timelimiting function - the custom for Fourier analysis, as discussed in [4].

⁶Refer to [11] for details about L^p stochastic processes.

⁷Justification for the choice of p is provided in [15].

⁸The reconstructions have been obtained using a modified version of the 50% section-overlap method of [19] (in particular, the same choice of multitaper time-bandwidth and zero-padding parameters). The modifications regard: the estimation of mode frequencies; and linear extrapolation of this nominal reconstruction at the record ends. The modifications and general reconstruction algorithm are all detailed in Algorithm 3 of [16]. The reconstruction is denoted by $\hat{x}^{(SGN)}$ in Section IV A of [16]. For $N = 6 \times 10^4$, the size of the grid of the zero-padded fast Fourier transform is 1.31072×10^5 . Refer to Section II of [16] for details of these parameter initializations.

⁹Details of the frequency calculations are specified in the section forthcoming; for now, remark that 14 Hz - a multiple of 7 Hz - is the alpha-band upper bound specified by [30].

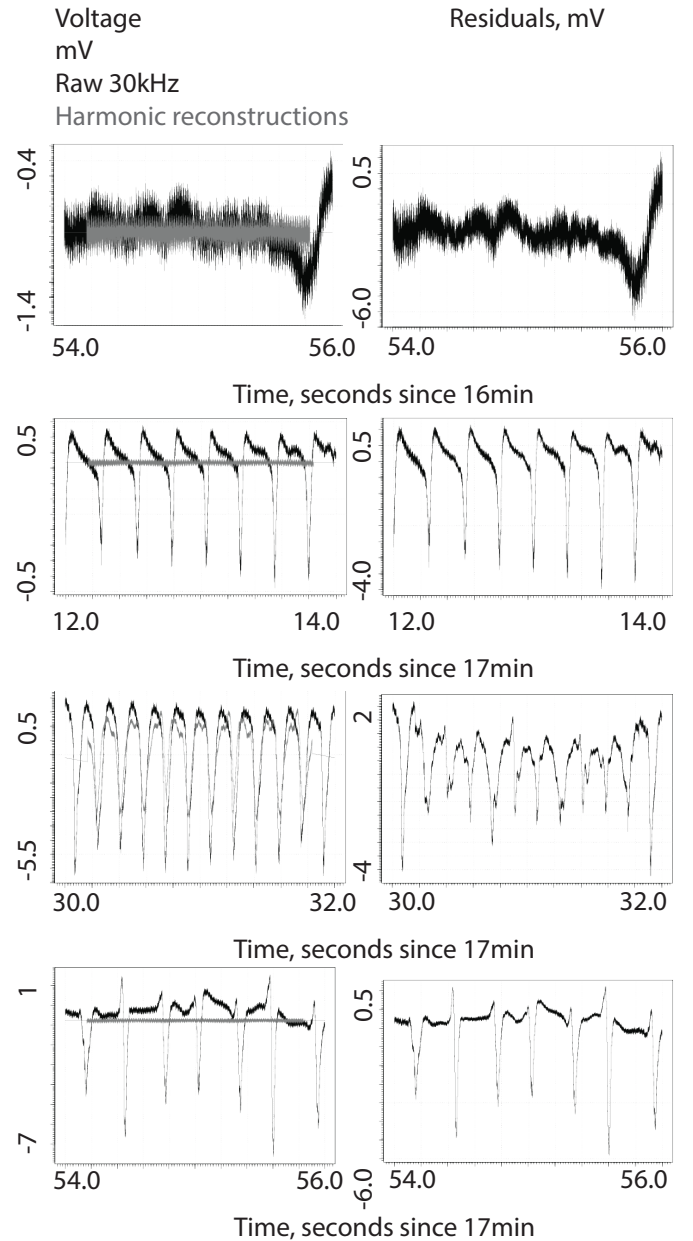


Fig. 1. A cosine-series signal accurately represents mean MEA-voltage in some epochs but not others. Left: a 30 kHz section trace (black) overlaid by a cosine-series reconstruction (grey). Right: residuals of the cosine-series reconstruction.

third plot row shows approximately 12 full troughs occurring between 30.0 and 31.8 s - and 12 cycles in 1.8 s yields 6.7 Hz. As for the ‘‘Ictal wavefront’’ and ‘‘Ictal discharges’’ epoch names, these have been chosen based on the terminology of [27]. The table also includes columns for the base time and the time interval of that plot row of Fig. 1 which the table row details. Mean voltage accurately explains the observed x -periodicity (first and third plot rows, with $x^{(SGN)}$ included in the ‘‘Dominant’’ column of Table I) whenever the grey $x^{(SGN)}$ -reconstruction trace: tracks the black x -trace; and has comparable amplitude to that of the x -trace fluctuations. In cases where $x^{(SGN)}$ does not so well explain x (i.e., second and fourth plot rows of Fig. 1), Table I identifies $X^{(NSE)}$ as

the main contributing X -component. In other words, it may well be possible to make the assumption that $X^{(NSE)}$ has nonzero mean signal and then add more of those modes to $x^{(SGN)}$ in the revised model; however, this would lead to a cosine series that is less sparse and so having higher estimation variance¹⁰.

TABLE I
THE EPOCHS OF AN MEA-VOLTAGE RECORD

Epoch	Base min	Interval s	Dominant
Alpha periodicity, early seizure	16	[54.0,56.0]	$x^{(SGN)}$
Ictal wavefront	17	[12.0,14.0]	$X^{(NSE)}$
Alpha periodicity, late seizure	17	[30.0,32.0]	$x^{(SGN)}$
Ictal discharges	17	[54.0,56.0]	$X^{(NSE)}$

Fig. 1 shows how the epochs of MEA-voltage during a human seizure can be identified simply using the cosine-series signal element of mean voltage. For the first row, x -points produce: a dense, black, central region; and a sequence of local minima and maxima more resolved in time. Absence of these minima and maxima in the corresponding residuals plot reveals these points to belong to $x^{(SGN)}$. For the third plot row, the smooth curvature of x in a time interval between sharp-trough events explains the good fit of $x^{(SGN)}$ (the grey and black curves line up). By contrast, remark the sharp x peaking that occurs in the second and fourth plot rows - it is said that X is anharmonic (i.e., its variability dominated by that of $X^{(NSE)}$) during the epochs of ictal wavefront and ictal discharges (second and fourth plot rows).

Plotting the frequency-domain signals that characterize the finite-dimensional distribution of X provides useful diagnostics to explain the functional behaviours observed in the plots of Fig. 1. To this end, consider the diagnostic plots of Fig. 2: whose four plot rows correspond to those of Fig. 1, and whose contents are as follows¹¹.

1) First column:

- Spectral power - multitaper jackknife mean estimates (black, [36]).
- Multitaper 95% confidence intervals (grey, [36]).

2) Second column:

- Multitaper F-statistic spectrum [35].
- Bonferoni $(1 - \frac{1}{N})$ level - horizontal line¹².

During the early-seizure alpha and ictal-wavefront epochs, the

¹⁰Details are provided in [15] about constructing a sparse cosine-series model for the autocorrelation function of $X^{(NSE)}$ - typically, a more efficient signal-processing method than simply adding more normal modes to $x^{(SGN)}$ whenever x contains sharp-edged waveforms.

¹¹The power-spectrum reconstructions have been obtained using the multitaper estimation scheme discussed in [15].

¹²Refer to [15] for details about the Bonferoni level. Algorithm 1 includes a data-adaptive step for test-threshold assignment that ensures at least a user-specified number (3 the default) of identified $x^{(SGN)}$ normal modes, but since the Bonferoni threshold satisfies the 3-detection criterion the threshold adaptation was unnecessary.

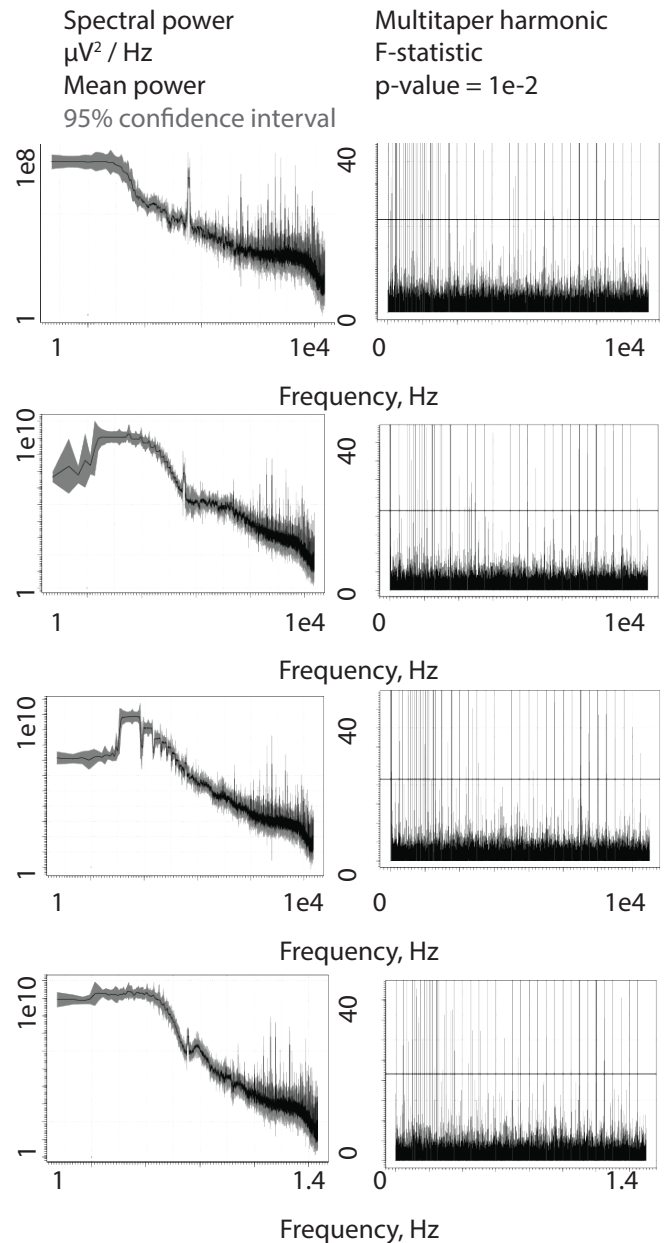


Fig. 2. The amplitudes and frequencies of mean-voltage normal modes are revealing about generative oscillations. Left: spectral power - jackknifed estimates of mean (black) and 95% confidence bounds (bounded grey region) of the multitaper spectral-power estimator - point-by-point across the non-negative part of the principal domain. Right: spectra of multitaper harmonic F-statistic values (99.998% the Bonferoni level, i.e. 10^{-2} p-value).

power spectrum (first and second plots, respectively) displays three notable features, as follows.

- 1) A 60 Hz spectral peak (alternating current¹³). This is the tallest peak in both plots, occurring midway along the frequency axis.
- 2) Conspicuous high-frequency spectral peaks right of the 60 Hz peak.
- 3) A log-linear decay indicative of red noise¹⁴

¹³Refer to Section 6.2.2 in [10].

¹⁴Refer to [7], [32] for a description of red noise.

As for the late-seizure alpha and ictal-discharge epochs, remark how the 60 Hz spectral peak disappears, but that the log-linear trend and high-frequency peaks remain similar to what they are for the other two epochs.

In the second column of Fig. 2, the F-statistic spectra reveal a plethora of level-99.99% peaks. The reason that the peak frequencies extend all the way out to the 30 kHz Nyquist rate is because no one of the considered time sections has pure-sinusoid periodicity; for example, even given the accurate fit in the third plot row of Fig. 1, there remains significant residual periodicity (refer to the residuals plot right of the 30 kHz-trace / fit overlay). That F-statistic peak height does not decay prior to the Nyquist rate is evidence that alpha periodicity enters the system as an alpha rhythm in the argument of the nonlinear system function.

B. Period Estimation for the Mean Signal

The multitaper F-statistic spectra in Fig. 2 revealed normal modes in $x^{(SGN)}$. For each of the early- and late-seizure alpha epochs, this section reveals further that the collection of identified normal modes corresponds to those of just a single cosine series - as opposed to the alternative, which is a sum of independent cosine series: each having unique fundamental frequency. In addition, the inferred fundamental frequency of $x^{(SGN)}$ in either epoch suggests the presence of an alpha-rhythm source. Table II displays both results and performance diagnostics of the estimation algorithm for fundamental frequency¹⁵. For fundamental-frequency inference the early-seizure alpha epoch (Table II, first row), both the table contents and estimation method are now described making use of Fig. 3, which itself includes the following.

- 1) **Top** Scatter plot (solid, blue diamonds) of mode frequency versus sequence index (the sequence indices being

$$\{1, 2, \dots, \check{J}_{SGN}\},$$

with \check{J}_{SGN} the number of identified mode frequencies and an integer estimate of J_{SGN} - “No. ID” in Table II). Solid, orange discs and table entries are discussed in the second list item below. Linear correlation occurs across a number of scatter-point clusters, as illustrated with the use of the plotted linear trendline (remark from the plot insert that $R^2 = 0.94$).

- 2) **Bottom** The same plot as the top one, except now with the following two changes so that all scatter points approximately correspond to just a single cosine series.
 - a) Dynamic scale expansion of the spacing between pairs of sequence indices (corresponding to harmonic indices - that is: integral multiples of a single fundamental frequency).
 - b) A zero-intercept constraint in the linear regression of identified frequencies on the harmonic indices.

Up to a sequence index of 21, the scatter points of the top plot (solid, blue diamonds) exhibit high linear correlation. So too, do the scatter points having sequence indices between 22 and 26 (the 22nd scatter point is

a changepoint for the slope; in both top and bottom plots a solid, orange disc is overlaid on the solid, blue diamond). To align both of these two scatter-point clusters, different trial spacings are introduced between sequence indices to produce trial harmonic indices. As seen in the bottom plot on either side of the orange disc: a 20-step spacing suffices (the 1(20) entry under the Table II “Changepoint (Steps)” column). Now, the first two clusters combined exhibit strong linear correlation; however, neither this cluster nor the cluster of remaining scatter points are collinear with the resulting linear trendline. Thus: sequence indices of the second cluster in the bottom plot are converted to harmonic indices by raising the sequence-index separation size from 1 to 15 (the 22(15) Table II entry). This action makes more of the scatter points collinear in total - and so brings the scatter points nearer the trendline on average. Next, the top plot is used to identify a third high-correlation cluster (sequence indices 27 through 37; solid, orange disc overlaid on the 37'th scatter point of both top and bottom plots) inside the larger cluster of remaining scatter points. Then, this third cluster is aligned with the first two of the bottom plot (the 27(80) Table II entry). The process is continued until all scatter points align both with each other and with the resulting trendline (remark from the plot insert that $R^2 = 0.998$).

TABLE II
FUNDAMENTAL-FREQUENCY CALCULATIONS FOR THE MEAN-VOLTAGE COSINE SERIES

Base min	Interval s	Frequency Hz	No. ID	Changepoint (Steps)	R^2
16	[54.0,55.8]	7.2	65	1(20), 22(15), 27(80), 38(40)	0.9983
17	[30.0, 31.8]	21.9	60	1(1), 7(20), 10(5), 24(15), 33(20)	0.9953

Fig. 4 displays the same contents as Fig. 3, except now for the late-seizure alpha epoch. The second row of Table II contains the relevant estimates and performance diagnostics. Given the high R^2 -value, it would appear that a single cosine series is adequate to explain the periodicity in mean voltage.

III. DISCUSSION

In Table II, 21.9 Hz is approximately three times the 7.2 Hz fundamental frequency; therefore, both of the associated cosine series have a 7 Hz fundamental frequency. The alpha band - (9, 14] Hz [30] - contains the basebands of several oscillations in temporal-lobe¹⁶, extracellular, electric potential whose spatial range is appreciable. Alpha oscillations are attributed

¹⁶Here, an oscillation is distinguished from a rhythm because the former is just an L^2 -demodulate of the generative, random neural data signal - there is no constraint about it being nonrandom or narrowband.

¹⁵For a detailed overview, refer to Algorithm 4 in [16].

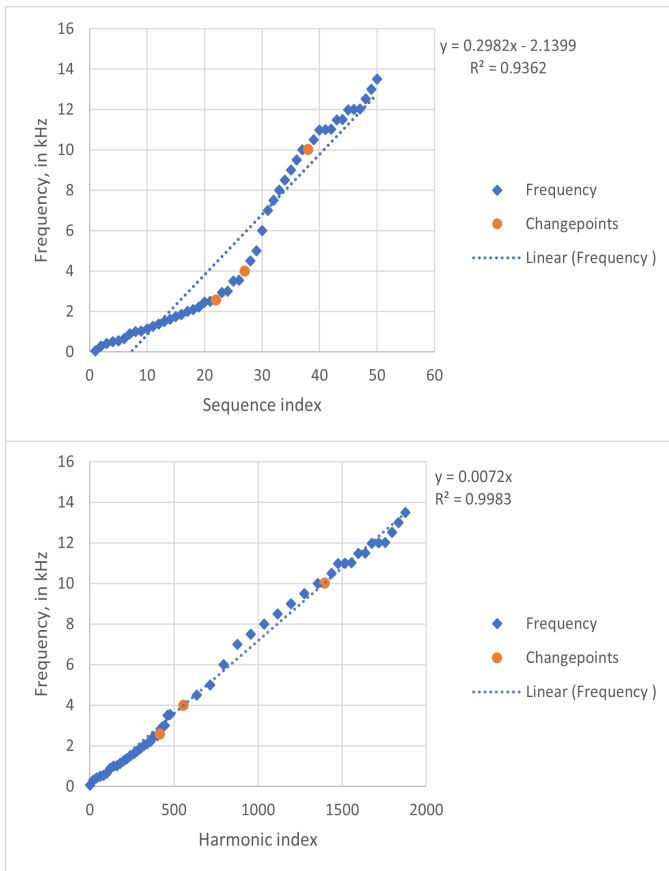


Fig. 3. Between them, mean-voltage mode frequencies in the early-seizure alpha epoch reveal a 7.2 Hz fundamental frequency. Top: Identified mode frequency vs. sequence index, given the training section that corresponds to the first row in Table I. Bottom: Same as the top, but now with scale expansions to sequence-index step size (resulting in harmonic indices, changepoints correspond to scale changes). Display box: fitted trendline model and the R^2 -value.

to the following connectivity dynamics during human seizure, and long range of the oscillations indicates that the temporal lobe during epileptic seizure is relatively transparent to 14 Hz oscillations.

- 1) During medial refractory seizures, MEA recordings reveal how the (4, 14) Hz oscillation accurately predicts action potential (AP) timing [40]¹⁷
- 2) Both during the wake and natural-sleep brain states, the [10, 20] Hz-oscillation is excited in the mesial temporal lobe [38]. In addition, [38] lists the following references that sighted a limbic-system 14 Hz normal mode during rapid eye movement (REM) sleep: [14], [22], [23].
- 3) Recent literature specifies a spindle as an $x_c^{(SGN)}$ -mode whose line power is approximately the average spectral mass in the [10, 15] Hz sigma frequency band during States 2,3 nonREM sleep¹⁸. In [38], 14 Hz is deemed characteristic of sleep spindles¹⁹: citing Fig. 6 of [3],

¹⁷For a complex survey of MEA-recordings including three cell strata, the number of cases where LFP successfully predicts spike timings falls from 26 down to 8 when shifting from the (4, 14) Hz band to the (14, 30) Hz band.

¹⁸Refer to Section 3.2.7 in [33]. Section 3.3.1 in that reference specifically considers: [1], [24]–[26], [37]

¹⁹The “spindle” term was coined in [13], and the phenomenon first identified in [2] - see [8] for an overview.

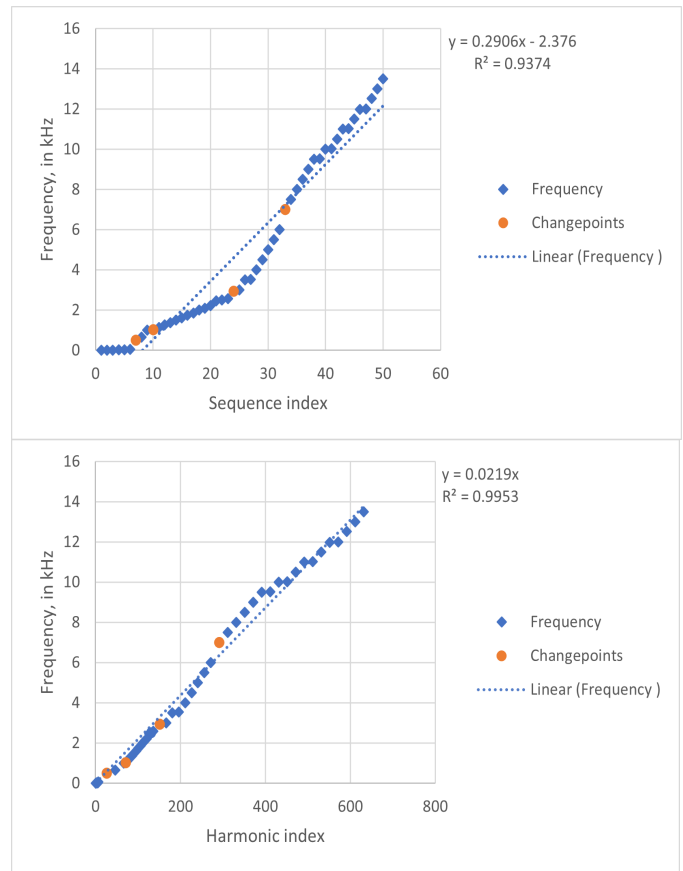


Fig. 4. Between them, mean-voltage mode frequencies in the late-seizure alpha epoch reveal a 21.9 Hz fundamental frequency. The same as Fig. 3, except now with the training section corresponding to the third row in Table I.

in which occurs an outstanding 14 Hz spectral peak in simultaneous electrode recordings of both the hippocampal gyrus and interior²⁰. Whereas [3] itself presents no evidence of 14 Hz spindles in electroencephalogram (EEG) recordings²¹, it does provide other evidence for long-range connectivity.

In [34], it is suggested that the spike-and-wave discharges in epilepsy during nonREM sleep might be generated in ways similar to spindles²²: in the same spirit for proposing biophysical models under a common-source hypothesis, it is here proposed that the mechanism responsible for the inferred 7 Hz oscillation arises in part due to the presence of an alpha rhythm. A candidate mechanism is the action of a nonlinear MEA system function on a 7 Hz wavepacket; [6] shows how the result is a 7 Hz cosine series²³.

²⁰Remarkable evidence for this 14 Hz power is also encountered in Fig. 5 of the more recent work, [8]: in the frontal and parietal cortices, coincident 14 Hz peaks occur during nonREM sleep.

²¹In more recent works, Section 3.3.1 in [33] states that the following works have indeed observed in EEG recordings large-scale propagation via an association between spindle voltage and sigma power: [8], [39].

²²In particular, refer to the spindle / spike-and-wave discharge comparison in Fig. 1 of [12].

²³The order, J_{SGN} , depends on how many derivatives the nonlinear system function has at the origin - a consequence of MacLaurin series expansions. The greater the number of derivatives, the smoother the system function.

IV. CONCLUSION

This manuscript has revealed that the sparse cosine-series modeling of mean MEA-voltage fails to explain the outstanding periodicity during epochs of ictal wavefronts and of ictal discharges. As such, rigorous dynamical modeling should include nonlinear and/or stochastic noise specification. It appears that the epochs of early- and late-seizure alpha periodicity both share a common 7 Hz source (suggesting the presence of a source alpha rhythm), but that a 7 Hz rhythm appears only as a driver for the MEA system function. This hypothesis precludes spatiotemporal localization of the source because more about the system function must be known before asserting that the plane-wave dynamics of a single source are generative of mean MEA-voltage.

ACKNOWLEDGMENT

F.A. Marshall thanks Prof. Mark Kramer, Ms. Emily Schlafly and Dr. Ani Wodeyar²⁴ for their contributions in discussions regarding the underlying theory and biophysics of cortical traveling waves received by MEA's.

ACRONYMS

AP	action potential. 5
EEG	electroencephalogram. 5
LFP	local field potential. 1, 5
MEA	microelectrode array. 1, 5, 6
NSE	noise. 2
REM	rapid eye movement. 5
SGN	signal. 2
SNR	signal-to-noise ratio. 1

REFERENCES

- [1] M. Beelke, L. Nobili, M.G. Baglietto, F. De Carli, A. Robert, E. De Negri, and F. Ferrillo. Relationship of sigma activity to sleep interictal epileptic discharges: a study in children affected by benign epilepsy with occipital paroxysms. *Epilepsy research*, 40(2-3):179–186, 2000.
- [2] H. Berger. Über das elektroencephalogram des menschen. sechste mitteilung. *Arch Psychiatr Nervenkr*, (99):555–574, December 1933.
- [3] M.A. Brazier. Studies of the EEG activity of limbic structures in man. *Electroencephalography and clinical neurophysiology*, 25(4):309–318, 1968.
- [4] D. R. Brillinger. *Time series: Data analysis and theory*, volume 36. Siam, 1981.
- [5] J. M. Diamond, B. E. Diamond, M. S. Trotta, K. Dembny, S. K. Inati, and K. A. Zaghoul. Travelling waves reveal a dynamic seizure source in human focal epilepsy. *Brain*, 144(6):1751–1763, 2021.
- [6] R. P. Feynman, R. B. Leighton, and M. Sands. *The Feynman Lectures on Physics; Vol. I*. Basic Books, 2010.
- [7] P. F. Fougere. On the accuracy of spectrum analysis of red noise processes using maximum entropy and periodogram methods: Simulation studies and application to geophysical data. *Journal of Geophysical Research: Space Physics*, 90(A5):4355–4366, 1985.
- [8] L. De Gennaro and M. Ferrara. Sleep spindles: an overview. *Sleep medicine reviews*, 7(5):423–440, 2003.
- [9] E. Hecht. Optics 4th edition. *Pearson: Addison Wesley*, 2002.

- [10] M. A. Kramer and U. T. Eden. *Case studies in neural data analysis: A guide for the practicing neuroscientist*. MIT Press, 2016.
- [11] V. Krishnan. *Nonlinear filtering and smoothing: An introduction to martingales, stochastic integrals and estimation*. Wiley Interscience, 1984.
- [12] N. Leresche, R. C. Lambert, A. C. Errington, and V. Crunelli. From sleep spindles of natural sleep to spike and wave discharges of typical absence seizures: Is the hypothesis still valid? *Pflügers Archiv-European Journal of Physiology*, 463(1):201–212, 2012.
- [13] A. L. Loomis, E. N. Harvey, and G. Hobart. Potential rhythms of the cerebral cortex during sleep. *Science*, 81(2111):597–598, 1935.
- [14] B.A. Malow, P.R. Carney, R. Kushwaha, and R.J. Bowes. Hippocampal sleep spindles revisited: Physiologic or epileptic activity? *Clinical Neurophysiology*, 110(4):687–693, 1999.
- [15] F. A. Marshall. *Advances in the detection and characterization of nonstationary processes: An application to riometers*. PhD thesis, Queen's University, Kingston, Ontario, 2020.
- [16] F. A. Marshall. Code Algorithms, 2023. GitHub. Last updated 2023. <https://github.com/fmarshall1/Multitaper-Harmonic-Analysis>.
- [17] F. A. Marshall. Multitaper–Harmonic–Analysis [source code], 2023. Last updated 2023. <https://github.com/fmarshall1/Multitaper-Harmonic-Analysis>.
- [18] F. A. Marshall, G. Takahara, and D. J. Thomson. A multitaper test for the detection of non-stationary processes using canonical correlation analysis. In *2018 IEEE Statistical Signal Processing Workshop (SSP)*, pages 702–706. IEEE, 2018.
- [19] F. A. Marshall, D. J. Thomson, G. Takahara, and R. A. Fiori. A multitaper model for quiet voltage in relative ionospheric opacity meters. In *2019 IEEE Global Conference on Signal and Information Processing (GlobalSIP)*. IEEE, 2019.
- [20] F. A. Marshall, D. J. Thomson, G. Takahara, R. A. Fiori, and D. W. Danskin. A characterization of periodicity in the voltage time series of a riometer. *Journal of Geophysical Research: Space Physics*, 2020.
- [21] L.-E. Martinet, G. Fiddymont, J.R. Madsen, E. N. Eskandar, W. Trucolo, U. T. Eden, S. S. Cash, and M. A. Kramer. Human seizures couple across spatial scales through travelling wave dynamics. *Nature communications*, 8(1):1–13, 2017.
- [22] J. Montplaisir, L. Leduc, M. Laverdiere, J. Walsh, and J.M. Saint-Hilaire. Sleep spindles in the human hippocampus: Normal or epileptic activity? *Sleep*, 4(4):423–428, 1981.
- [23] T. Nakabayashi, S. Uchida, T. Maehara, N. Hirai, M. Nakamura, H. Arakaki, H. Shimisu, and Y. Okubo. Absence of sleep spindles in human medial and basal temporal lobes. *Psychiatry and clinical neurosciences*, 55(1):57–65, 2001.
- [24] L. Nobili, M. G. Baglietto, M. Beelke, F. De Carli, E. Veneselli, and F. Ferrillo. Temporal relationship of generalized epileptiform discharges to spindle frequency activity in childhood absence epilepsy. *Clinical neurophysiology*, 112(10):1912–1916, 2001.
- [25] L. Nobili, M.G. Baglietto, M. Beelke, F. De Carli, E. De Negri, R. Gaggero, G. Rosadini, E. Veneselli, and F. Ferrillo. Distribution of epileptiform discharges during nREM sleep in the CSWSS syndrome: Relationship with sigma and delta activities. *Epilepsy research*, 44(2-3):119–128, 2001.
- [26] L. Nobili, F. Ferrillo, M.G. Baglietto, M. Beelke, F. De Carli, E. De Negri, G. Schiavi, G. Rosadini, and M. De Negri. Relationship of sleep interictal epileptiform discharges to sigma activity (12–16 Hz) in benign epilepsy of childhood with rolandic spikes. *Clinical neurophysiology*, 110(1):39–46, 1999.
- [27] C. A. Schevon, S. Tobochnik, T. Eissa, E. Merricks, B. Gill, R. R. Parrish, L. M. Bateman, G. M. McKhann Jr, R. G. Emerson, and A. J. Trevelyan. Multiscale recordings reveal the dynamic spatial structure of human seizures. *Neurobiology of disease*, 127:303–311, 2019.
- [28] E. D. Schlafly and M. A. Kramer. Human seizure MEA, 2022. Boston College, Accessed: 2022, Last updated 2022-05-25.
- [29] E. D. Schlafly, F. A. Marshall, E. M. Merricks, U. T. Eden, S. S. Cash, C. A. Schevon, and M. A. Kramer. Multiple sources of fast traveling waves during human seizures: Resolving a controversy. *Journal of Neuroscience*, 42(36):6966–6982, 2022.
- [30] Z. Shi, D. M. Wilkes, P.-F. Yang, F. Wang, R. Wu, T.-L. Wu, L. M. Chen, and J. C. Gore. On the relationship between MRI and local field potential measurements of spatial and temporal variations in functional connectivity. *Scientific reports*, 9(1):1–11, 2019.
- [31] L. E. Sinclair, F. A. Marshall, and R. Fortin. Reconstruction of the spatial distribution of radioactive contamination from aerial survey and from a stationary array of directional detectors. In *2015 IEEE Nuclear Science Symposium and Medical Imaging Conference (NSS/MIC)*, pages 1–4. IEEE, 2015.

²⁴Computational Neurodata and Modeling Lab, Mathematics and Statistics, Boston University.

- [32] V. Solo. Intrinsic random functions and the paradox of $1/f$ noise. *SIAM Journal on Applied Mathematics*, 52(1):270–291, 1992.
- [33] E. R. S. Spencer. *Biomarker discovery and statistical modeling with applications in childhood epilepsy and Angelman syndrome*. PhD thesis, Boston University, 2021.
- [34] J. Summer and A. Rehman. Sleep spindles, 2022. Viewed September 29, 2022, Updated April 25, 2022.
- [35] D. J. Thomson. Quadratic-inverse spectrum estimates: Applications to palaeoclimatology. *Phil. Trans. R. Soc. Lond. A*, 332(1627):539–597, 1990.
- [36] D. J. Thomson. Jackknifing multitaper spectrum estimates. *IEEE Signal Processing Magazine*, 24(4):20–30, 2007.
- [37] M. A. Tucker and W. Fishbein. The impact of sleep duration and subject intelligence on declarative and motor memory performance: How much is enough? *Journal of sleep research*, 18(3):304–312, 2009.
- [38] S. Uchida, T. Maehara, N. Hirai, Y. Okubo, and H. Shimizu. Cortical oscillations in human medial temporal lobe during wakefulness and all-night sleep. *Brain research*, 891(1-2):7–19, 2001.
- [39] E. J. Wamsley, M. A. Tucker, A. K. Shinn, K. E. Ono, S. K. McKinley, A. V. Ely, D. C. Goff, R. Stickgold, and D. S. Manoach. Reduced sleep spindles and spindle coherence in schizophrenia: mechanisms of impaired memory consolidation? *Biological psychiatry*, 71(2):154–161, 2012.
- [40] S. Zanos, T. P. Zanos, V. Z. Marmarelis, G. A. Ojemann, and E. E. Fetz. Relationships between spike-free local field potentials and spike timing in human temporal cortex. *Journal of neurophysiology*, 107(7):1808–1821, 2012.



François A. Marshall was born in London, England in 1990. He received: B.S. (Theoretical Physics, 2012) and M.S. (Medical Imaging Physics, 2014) degrees from Carleton University, Ontario, Canada; and a Ph.D. degree (Applied Mathematics, 2020) from Queen's University, Ontario, Canada.

During the M.Sc., he was Research Assistant with Natural Resources Canada (Nuclear Emergency Response Team). In Winter 2019, he was Teaching Fellow for “STAT 464/864 Time

Series Analysis” at Queen's University. From 2020 to 2022, he was a Postdoctoral Associate with Boston University Mathematics and Statistics. From October to December, 2022: he was a Visiting Scholar at Boston University (Neuromodeling and Data Lab, Mathematics and Statistics). He is first author on: [18], [20]; and second author on [31]. His research interests include: time-series and spectral analyses; stochastic processes and Monte Carlo; probability theory and analysis; and neuroscience.

Dr. Marshall is Secretary of Statistical Society of Canada (SSC) Student and Recent Graduates Committee and Secretary of SSC Probability Section. He is a member of: American Epilepsy Society; American Geophysical Union; Royal Statistical Society; and SSC (Statistical Society of Ottawa). In 2019, he was a recipient of the SSC Probability Section Student Research Presentation Award.